General Disclaimer

One or more of the Following Statements may affect this Document

- This document has been reproduced from the best copy furnished by the organizational source. It is being released in the interest of making available as much information as possible.

- This document may contain data, which exceeds the sheet parameters. It was furnished in this condition by the organizational source and is the best copy available.

- This document may contain tone-on-tone or color graphs, charts and/or pictures, which have been reproduced in black and white.

- This document is paginated as submitted by the original source.

- Portions of this document are not fully legible due to the historical nature of some of the material. However, it is the best reproduction available from the original submission.

Produced by the NASA Center for Aerospace Information (CASI)

X-641-70-393
PREPRINT
NASA TM X- 65381

X-RAY EXCITED LMM ANGER SPECTRA OF COPPER, NICKEL, AND IRON

L. I YIN
E. YELLIN
I. ADLER

OCTOBER 1970

NOV 1970
RECEIVED
NASA STI FACILITY
INPUT BRANCH

GSFC
GODDARD SPACE FLIGHT CENTER
GREENBELT, MARYLAND

FACILITY FORM 602
N71-10584 (ACCESSION NUMBER)
27 (PAGES)
TMX 65381 (NASA CR OR TMX OR AD NUMBER)
(THRU)
63 (CODE)
24 (CATEGORY)

X-Ray Excited LMM Auger Spectra of Copper, Nickel, and Iron

L. I Yin, E. Yellin, and I. Adler

ABSTRACT

Photoelectron and Auger electron spectra are both obtained with x-ray excitation. Using the photoelectron spectra as internal energy standards, the energies of the prominent LMM Auger lines in Cu, Ni, and Fe have been accurately determined. In addition, the photoelectron spectra provide a measure of the vacancy distribution created by the x-rays among the three L-subshells. Thus, knowing both the energy values and the vacancy distribution, we have assigned the three prominent Auger lines of Cu, Ni, and Fe to be of type L_3MM rather than L_2MM.

I. INTRODUCTION

KLL Auger spectra have been investigated at length both theoretically and experimentally,[1,2] but information on the Auger transitions involving outer shells has been rather meager. Noteworthy exceptions in this regard are the works of Mehlhorn[3-6], Asaad[6], and Carlson and Krauss[7,8], as well as Siegbahn et al.[2] on the L- and M-Auger spectra of the noble gases Argon and Krypton. Recently, Harris[9,10] obtained electron-excited Auger spectra with enhanced signal-to-noise ratios by taking the derivative of the electron energy distribution. Subsequently this method of signal-to-noise enhancement was adopted in the low energy electron diffraction (LEED) apparatus[11-13] to produce useful Auger spectra. Because of the low energy (<3 keV) of the incident electrons in such LEED-Auger systems, for elements with medium or high atomic numbers, mostly Auger transitions involving outer shells are observed. Current efforts to explore the potential usefulness of such spectra in the study of surfaces, chemical effects, and elemental analysis have given impetus to, and intensified interest in, the systematic survey of outer shell Auger Transitions[14]. Underlying the observation and correct indexing of such spectra are the also theoretically pertinent quantities such as Auger and Coster-Kronig yields and transition rates.

In this paper the LMM Auger spectra of Cu, Ni, and Fe obtained by low energy x-ray excitation will be examined and the results compared with results obtained by electron-excitation[12,14]. The most important difference between

electron-excited and x-ray-excited electron spectra lies in the fact that only the Auger lines are characteristic of the sample in the former case, whereas in x-ray excited spectra both photoelectron lines and Auger lines are characteristic of the sample. Because the position of the photoelectron lines is accurately known, an internal energy calibration standard exists for the lesser known Auger lines. Another difference in the present context is, because of the inherently high signal-to-background ratio of x-ray-excited spectra, no differentiation of the energy distribution is necessary. The peak position can be determined directly from the spectra rather than from the slope of the differentiated spectra. Based on present data, a somewhat different assignment for the prominent LMM transitions in Cu, Ni, and Fe will be presented and discussed.

II. EXPERIMENTAL METHOD

The detailed features of the instrumentation used in this experiment have been reported elsewhere[15]. An oil-diffusion pump system operating at 10^{-6} torr houses a Deslattes[16]-type soft x-ray tube and a hemispherical electrostatic analyzer. The electrons are pulse-counted by a channel electron-multiplier; a multichannel analyzer operated in the multiscaler mode displays the energy spectra. Two modes of operation are employed. In one, the sample and the entrance slit of the spectrometer are kept at ground while the potential across the hemispheres is varied by a linear voltage-ramp generator. In this mode of

operation the percentage energy resolution $\Delta E/E$ stays constant, thus it is used to observe the overall coarse features of the spectrum. In the other mode, the spectrometer is set to accept 200-eV electrons while the voltage-ramp is used to supply a varying retarding potential on the sample[17]. Because the absolute energy resolution ΔE is constant in this mode, it is useful for obtaining more precise measurements of the finer features of a spectrum. A block diagram of the instrumentation is shown in Fig. 1.

Samples were made from pure copper, nickel, and iron foils, and the sample surfaces were routinely cleaned by Argon- or Nitrogen-ion bombardment. Without such treatment, it was difficult to obtain any spectra of reasonable quality.

Since the position of Auger lines, unlike the position of photoelectron lines, is independent of the energy of the exciting radiation, both Al $K_{\alpha_{1,2}}$ (1487 eV) and Mg $K_{\alpha_{1,2}}$ (1254 eV) x-rays were used to ensure that the photoelectron and Auger lines would be clearly distinguishable from each other. These different x-ray sources also served as two independent energy calibration standards for the Auger lines.

III. RESULTS

The overall spectra of Cu as excited by Al $K_{\alpha_{1,2}}$ and Mg $K_{\alpha_{1,2}}$ x-rays are shown in Figs. 2A and 2B on a common energy axis. These spectra were obtained by scanning the spectrometer as described by mode A of Fig. 1. With

the Al $K_{\alpha_{1,2}}$ x-rays, photoelectron lines from the L_I, L_{II}, L_{III}, M_I, and $M_{II,III}$ shells, and the 3d4s band of Cu, are all clearly displayed (Fig. 2A). Because of their lower energies, and consequently lower escape probabilities from the sample, the L photoelectron lines excited by the Mg $K_{\alpha_{1,2}}$ x-rays are less clear (Fig. 2B). As expected, the features of the prominent Auger peaks remain unchanged in both spectra.

In Fig. 2, the photoelectron lines appear on both the low and high energy sides of the Auger peaks; therefore they serve as excellent energy standards for the precise location of the Auger peaks. For this purpose, the following procedure was adopted: The three regions containing $L_{II,III}$ photoelectrons, Auger, and M photoelectrons were scanned separately under high resolution by varying the retarding potential on the sample and setting the spectrometer to accept 200-eV electrons. These spectra are displayed in Figs. 3, 4, and 5 respectively. The tabulated binding energy of L_{III} was taken from Reference 2 to compute the correct energy of the L_{III} photoelectron line. This value was then assigned to the L_{III} line in Fig. 3. In this fashion, the work function of the spectrometer was implicitly accounted for. Using the L_{III} peak as a reference, the positions of all the other photoelectron peaks were deduced from only the experimental data shown in Figs. 3 and 5. These peaks were then compared with theoretical values to reassure that the instrumentation had linearity and had functioned properly. Instrumental accuracy both below and above the Auger region thus established, the energies of the Auger peaks themselves (Fig. 4)

could be determined and error limits assigned. Error limits are caused mainly by the broadness of the Auger peaks, and in some cases poor counting statistics. For redundancy, the same procedure was repeated for the spectra excited by Mg $K_{\alpha_{1,2}}$ x-rays. The analogous set of Ni spectra shown in Figs. 6-8 was also analyzed in the same way. Statistical fluctuations made it difficult to assign values to the fine structures in the Auger spectra other than to the one labelled as A4 in Ni and Cu.

The Al $K_{\alpha_{1,2}}$ excited Fe spectrum is shown in Fig. 9. Because of the use of Al $K_{\alpha_{1,2}}$ radiation, there is an unfortunate overlap between the L_I photoelectron peak of Fe (641 eV) and the A2 Auger peak (644 eV). However, judging from the relative intensities of L_{II}, L_{III} /L_I in Cu and Ni, the L_I photoelectron peak should cause little distortion on the position of the A2 Auger peak. Due to the high background, the A4 Auger peak cannot be seen with Al $K_{\alpha_{1,2}}$ x-rays. Unfortunately, in our case, the Mg $K_{\alpha_{1,2}}$ x-rays did not give sufficient intensity to provide a high quality Fe Auger spectrum.

IV. DISCUSSION

The energies of the LMM Auger peaks established in our experiment are, in general, lower than those obtained through electron-excitation[12,14] as shown in Table I.

The following equation [18,19] is often used to calculate the approximate energies of the various Auger transitions.

$$E_{LXY}(Z) = E_L(Z) - E_X(Z) - E_Y(Z)$$

$$- \Delta Z \left[E_Y(Z+1) - E_Y(Z)\right] \qquad (1)$$

where $E_{LXY}(Z)$ is the energy of the LXY Auger electron of an atom with atomic number Z, and $E_L(Z)$, $E_X(Z)$ and $E_Y(Z)$ are, respectively, the binding energies of the atomic levels L, X, and Y of the neutral atom, and $E_Y(Z + 1)$ is the binding energy of the Y level of the atom one atomic unit higher. The last term which includes the "effective incremental charge"[18], ΔZ, is used to account for the increase in binding energy of the Y level when one electron is missing from the X shell. This ΔZ value is empirically determined and usually falls between 0.7 and 1.3[20]; the average can be taken as 1. In the present context, because no ΔZ value is available, it is given an average value of 1 which reduces equation (1) to the familiar form[21]:

$$E_{LXY}(Z) = E_L(Z) - E_X(Z) - E_Y(Z+1)\,. \qquad (2)$$

(It should be pointed out that final assignment of the Auger lines based on the present data is not affected even when ΔZ is chosen to be 0, although the energy agreement is much poorer.)

A table is made up of all the possible LMM transitions in Cu, Ni, and Fe using Equation (2). Strictly speaking, this form of classification of Auger transitions implies j-j coupling of the final vacancies in the outer shells. However, because of the relatively coarse resolution and insufficient counting statistics of the present data, it is possible to assign correctly only the most prominent Auger lines to a given Auger group. This form of classification should be adequate.[19]

Table II shows that, for all the samples, A1 and A3 peaks can be unambiguously assigned to the transitions $L_3M_{2,3}M_{2,3}$ and $L_3M_{4,5}M_{4,5}$ respectively. A2 is closer in energy to $L_1M_1M_1$ than $L_3M_{2,3}M_{4,5}$ when $E_{M_{4,5}}(Z+1)$ is used to calculate the energy of $L_3M_{2,3}M_{4,5}$ transition. But when $E_{M_{2,3}}(Z+1)$ is used, (it is equivalent to writing $L_3M_{4,5}M_{2,3}$ as shown in Table II), A2 becomes equally close to $L_1M_1M_1$ and $L_3M_{2,3}M_{4,5}$ for Cu and Ni, and closer to $L_3M_{2,3}M_{4,5}$ for Fe. A4 agrees equally well with either $L_1M_{2,3}M_{2,3}$ or $L_2M_{4,5}M_{4,5}$ in Cu and Ni. Despite these seeming ambiguities, A2 is assigned to be $L_3M_{2,3}M_{4,5}$ and A4 to be $L_2M_{4,5}M_{4,5}$ for the following reasons: In a specific experimental geometry, at a given x-ray energy, and for a given atomic species, the intensity of a photoelectron line depends on several factors — the photoelectric cross section of the shell or subshell from which the electron is

ejected, the angular distribution of the ejected photoelectrons from that shell, the escape probability of photoelectrons from the sample with the ejected kinetic energy, and the detection efficiency of the spectrometer-detector system for electrons with this energy. In the case of L_{II} and L_{III} photoelectrons with almost equal kinetic energies, most of the factors mentioned above are also equal. Therefore, their relative intensities give a qualitative indication of their relative photoelectric cross sections. However, the fact that the L_{II} line is superposed on the low energy continuum of the L_{III} line gives an exaggerated indication of high intensity to L_{II}. Thus, our data indicate that at Al $K_{\alpha_{1,2}}$ x-ray energies, the L_{III} photoelectric cross section is about a factor of 2 larger than that of the L_{II} shell in Cu, Ni, and Fe. The kinetic energies of the L_I photoelectrons are about 150 eV to 200 eV lower than those of L_{II} and L_{III}; their escape probability, therefore, is also expected to be lower. It is quite obvious from Figs. 2 and 6 that, even allowing for the reduced escape probability, our data show that the photoelectron intensity of L_I is far below that of L_{II} and L_{III}. This is in agreement with other experimental[22] data and theoretical[23] calculations where the $L_I/L_{II} + L_{III}$ ratio in the region of our x-ray energy and atomic number is expected to be about 1/5.5. Therefore, it can be concluded from these photoelectron spectra that among the three L shells most of the ionizations (perhaps 85%) take place in the L_{II} and L_{III} shells, and that the L_{III} shell is about 2 times more highly ionized than the L_{II} shell. Furthermore, since practically all the L vacancies will be filled in this Z-region via Auger or

Coster-Kronig transitions[24], one expects the L_3MM Auger transitions to predominate strongly over those of L_2MM; the L_1MM transitions should be barely observable. Based on these observations A2 is assigned to be $L_3M_{2,3}M_{4,5}$ rather than $L_1M_1M_1$, and A4 to be $L_2M_{4,5}M_{4,5}$ rather than $L_1M_{2,3}M_{2,3}$.

One must mention in this connection the $L_1L_{2,3}M_{4,5}$ Coster-Kronig transitions. This is another mechanism which tends to suppress even further the L_1MM intensity and enhance the L_3MM/L_2MM intensity ratio. In this region of atomic number where Coster-Kronig transitions of the $L_1L_{2,3}M_{4,5}$ type are energetically possible, the transition rates are much higher than the L_1MM Auger rates[24]. Thus, it is expected that the majority of the vacancies created in the L_I-shell will be filled by an L_{II} or L_{III}-shell (rather than an M-shell) electron, and an $M_{4,5}$-shell electron will be ejected in the process. This will shift the original photoelectric vacancy distribution to favor the L_{II} and L_{III}-shells even more. Callan[25] has shown that the total $L_1L_{2,3}M_{4,5}$ Coster-Kronig rates essentially vary linearly with atomic number in this region. In addition, he has shown that the partial rate of $L_1L_3M_{4,5}$ is about twice that of $L_1L_2M_{4,5}$[26]. This further enhances the L_{III}/L_{II} vacancy ratio and, consequently, the L_3MM/L_2MM Auger intensity ratio. Although the L_2MM and L_3MM Auger transitions following a Coster-Kronig transition of the $L_1L_{2,3}M_{4,5}$ type will have a slightly higher energy due to the initially doubly-ionized atom, the amount of this shift will be small and probably not resolvable in the present experiment.

V. CONCLUSION

Using the available photoelectron spectra as energy standards, as well as a measure of the relative ionization cross-sections among the three L-subshells, the energies of the three prominent Auger lines in Cu, Ni, and Fe have been determined and assigned to be the transitions $L_3M_{2,3}M_{2,3}$, $L_3M_{2,3}M_{4,5}$, and $L_3M_{4,5}M_{4,5}$. (A fourth small Auger peak was assigned to the transition $L_2M_{4,5}M_{4,5}$.) This differs from the L_2MM assignment obtained by electron-excitation[12,14]. The difference may be instrumental in origin or it may lie in a different relative ionization cross-section among the L-subshells under electron-excitation. However, even with electron-excitation, at electron energies about twice that of the L-shell binding energies the L_I:L_{II}:L_{III} vacancy ratio is expected to be essentially (to within 10%) that of the electron population ratio of 1:1:2[27]. This ratio will in turn favor L_3MM transitions over those of L_2MM. During the writing of this paper, we obtained a chart of Auger electron energies based on electron-excitation data prepared recently by Y. E. Strausser and J. J. Uebbing of Varian Associates. The energies of their Auger lines, judging from the logarithmic scale of the chart, seem to be comparable to our values; they are given the same assignment as ours. The discrepancy between their chart and references 12 and 14 puts futher emphasis on the need for additional information to serve as criteria in assigning Auger transitions. The data presented in this paper show that such additional information is readily available from the photoelectron spectra. Further and more systematic study

of the LMM Auger lines using x-ray excitation under higher resolution and higher intensities is hopefully recommended.

VI. ACKNOWLEDGMENT

We are happy to express our gratitude to E. J. Callan for making reference 26 available to us, and to K. Omidvar and J. R. Cuthill for helpful discussions.

REFERENCES

1. K. Siegbahn Ed. "Alpha-, Beta- and Gamma-Ray Spectroscopy", Vol. 2, Chapter XXV, North-Holland Publishing Co., Amsterdam, (1966)
2. K. Siegbahn et al. "ESCA", Chapter VI, Technical Report AFML-TR-68-189 (1968)
3. W. Mehlhorn, Zeit. Physik 160, 247 (1960)
4. W. Mehlhorn, Zeit, Physik 187, 21 (1965)
5. W. Mehlhorn and D. Stalherm, Zeit. Physik 217, 294 (1968)
6. W. N. Asaad and W. Mehlhorn, Zeit. Physik 217, 304 (1968)
7. T. A. Carlson and M. O. Krause, Phys. Rev. Letters 14, 390 (1965)
8. T. A. Carlson and M. O. Krause, Phys. Rev. Letters 17, 1079 (1966)
9. L. A. Harris, G. E. Res. Dev. Report #67C201 (1967)
10. L. A. Harris, J. Appl. Phys. 39, 1419 and 1428 (1968)
11. R. E. Weber and W. T. Peria, J. Appl. Phys. 38, 4355 (1967)
12. P. W. Palmberg and T. N. Rhodin, J. Appl. Phys. 39, 2425 (1968)
13. P. W. Palmberg, Appl. Phys. Letters 13, 183 (1968)
14. T. W. Haas, J. T. Grant and G. J. Dooley, Phys. Rev. B1, 1449 (1970)
15. L. I Yin, I. Adler and R. Lamothe, Appl. Spect. 23, 41 (1969)
16. R. D. Deslattes and B. G. Simson, Rev. Sci. Instr. 37, 753 (1966)
17. B. L. Henke and R. E. Lent, Adv. in X-Ray Analysis 12, 480 (1969)
18. I. Bergström and R. D. Hill, Arkiv Fysik 8, 21 (1954)

19. M. A. Listengarten, Izv. Akad. Nauk SSSR 24, 1041 (1960); Trans. Bull. Akad. Sci. USSR (Phys. Ser.) 24, 1050 (1960)

20. L. H. Toburen and R. G. Albridge, Nuc. Phys. A90, 529 (1967)

21. E. H. S. Burhop, "The Auger Effect and Other Radiationless Transitions", Cambridge Univ. Press (1952)

22. See p. 160 of reference 2

23. M. A. Blokhin, "The Physics of X Rays" Chapter IV, AEC-tr-4502 (1957)

24. R. W. Fink, R. C. Jopson, Hans Mark and C. D. Swift, Revs. Mod. Phys. 38, 513 (1966)

25. E. J. Callan, Revs. Mod. Phys. 35, 524 (1963)

26. E. J. Callan, Proceedings of International Conference, Warsaw, 398 (1963)

27. K. Omidvar, to be published in J. Phys. B

TABLE I

Comparison of the prominent LMM Auger electron energies obtained by x-ray excitation (this work) and by electron-excitation[12,14].

Element	Auger peak designation	Refs. 12, 14 eV	This work eV
Fe	A1	605	593±3
	A2	655	644±3
	A3	710	704±2
Ni	A1	720	710±3
	A2	790	775±2
	A3	860	847±2
	A4		864±2
Cu	A1	795	769±3
	A2	875	839±2
	A3	950	919±2
	A4		937±2

TABLE II

Comparison of calculated LMM Auger energies using Equation (2) with the experimental values of this work. Numbers in bracket show possible assignment from energy alone but discarded owing to other considerations as discussed in the text. *The experimental value of this line agrees better with the calculated value in which $E_{M_{2,3}}(Z + 1)$ is used rather than $E_{M_{4,5}}(Z + 1)$.

Peak desig.	Transition	Calc. Cu	Exp'l Cu	Calc. Ni	Exp'l Ni	Calc. Fe	Exp'l Fe
A2	$L_1 M_1 M_1$	841	(839)	776	(775)	650	(644)
	$L_1 M_1 M_{2,3}$	890		822		691	
	$L_1 M_1 M_{4,5}$	969		894		748	
A4	$L_1 M_{2,3} M_{2,3}$	936	(937)	866	(864)	730	
	$L_1 M_{2,3} M_{4,5}$	1015		938		787	
	$L_1 M_{4,5} M_{4,5}$	1087		1003		837	
	$L_2 M_1 M_1$	695		640		527	
	$L_2 M_1 M_{2,3}$	744		686		568	
	$L_2 M_1 M_{4,5}$	823		758		625	
	$L_2 M_{2,3} M_{2,3}$	790		730		607	
	$L_2 M_{2,3} M_{4,5}$	869		802		664	

Peak desig.	Trans-ition	Calc. Cu	Exp'l Cu	Calc. Ni	Exp'l Ni	Calc. Fe	Exp'l Fe
A4	$L_2M_{4,5}M_{4,5}$	941	937	867	864	714	
	$L_3M_1M_1$	675		623		514	
	$L_3M_1M_{2,3}$	724		669		555	
	$L_3M_1M_{4,5}$	803		741		612	
A1	$L_3M_{2,3}M_{2,3}$	770	769	713	710	594	593
A2	$*L_3M_{2,3}M_{4,5}$	849	839	785	775	651	644
A3	$L_3M_{4,5}M_{4,5}$	921	919	850	847	701	704
A2	$*L_3M_{4,5}M_{2,3}$	842	839	777	775	644	644

FIGURE CAPTIONS

Fig. 1 Block diagram of instrumentation. Mode A. Scanning the spectrometer, $\Delta E/E$ is constant. Mode B. Scanning the sample, ΔE is constant.

Fig. 2 Overall electron spectrum of Cu, scanning the spectrometer. 2A. Al $K_{\alpha_{1,2}}$ excitation. 2B. Mg $K_{\alpha_{1,2}}$ excitation.

Fig. 3 L_{II} and L_{III} photoelectron lines of Cu (Al $K_{\alpha_{1,2}}$). Scanning the sample.

Fig. 4 Cu Auger electron lines. Scanning the sample.

Fig. 5 M photoelectron lines of Cu (Al $K_{\alpha_{1,2}}$). Scanning the sample.

Fig. 6 Overall electron spectrum of Ni (Al $K_{\alpha_{1,2}}$). Scanning the spectrometer.

Fig. 7 L_{II}, L_{III} photoelectron lines and Al, A2 Auger lines of Ni (Al $K_{\alpha_{1,2}}$). Scanning the sample.

Fig. 8 Ni Auger electron lines. Scanning the sample.

Fig. 9 L_{II}, L_{III} photoelectron lines and the Auger lines of Fe (Al $K_{\alpha_{1,2}}$). Scanning the sample.

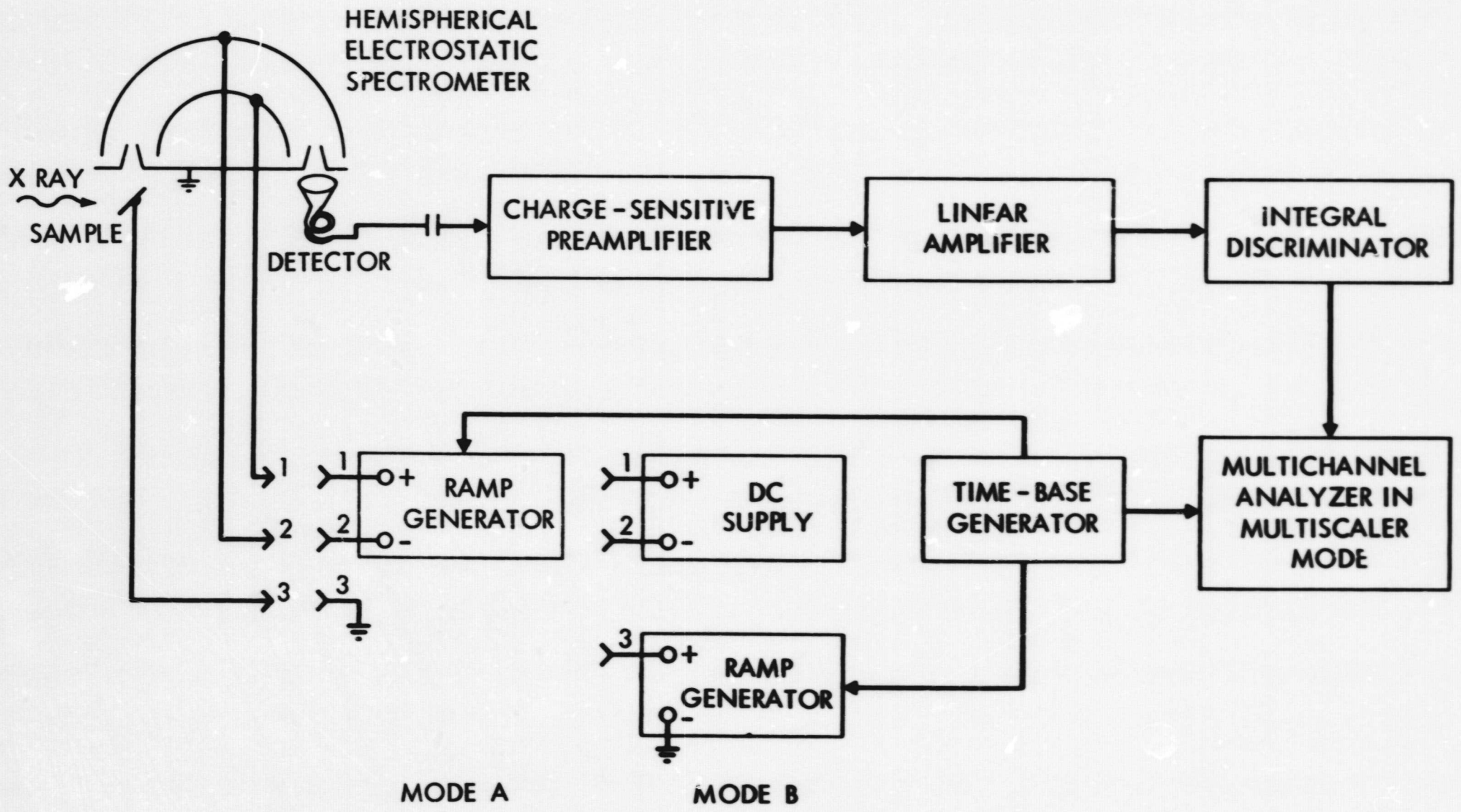
HEMISPHERICAL
ELECTROSTATIC
SPECTROMETER
X RAY
SAMPLE
DETECTOR
CHARGE - SENSITIVE
PREAMPLIFIER
LINEAR
AMPLIFIER
INTEGRAL
DISCRIMINATOR
1
2
3
RAMP
GENERATOR
DC
SUPPLY
TIME - BASE
GENERATOR
MULTICHANNEL
ANALYZER IN
MULTISCALER
MODE
RAMP
GENERATOR
MODE A
MODE B

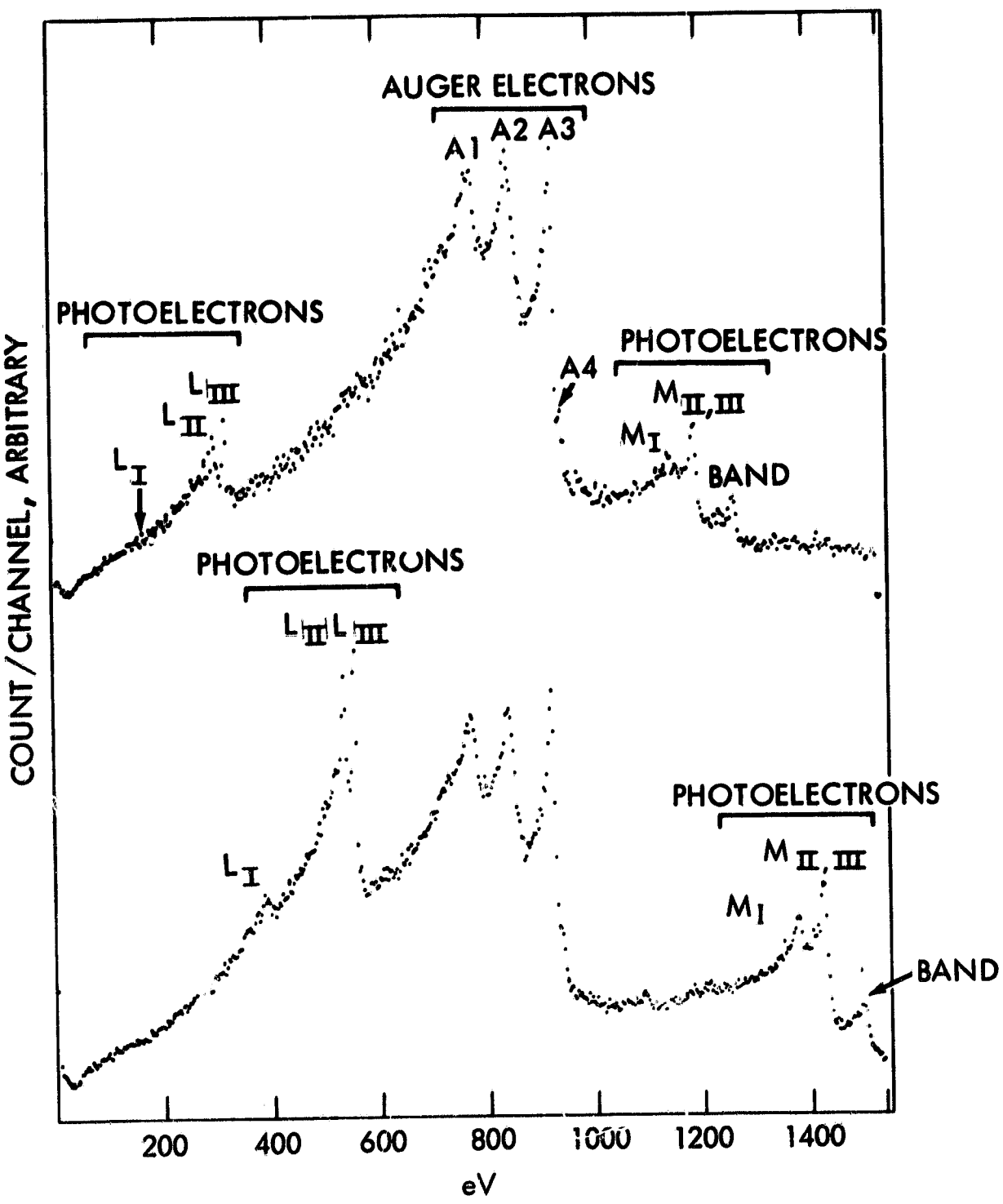
AUGER ELECTRONS
A1
A2 A3
PHOTOELECTRONS
PHOTOELECTRONS
A4
$M_{II,III}$
M_I
BAND
L_{III}
L_{II}
L_I
PHOTOELECTRONS
L_{II} L_{III}
PHOTOELECTRONS
$M_{II,III}$
M_I
BAND
L_I
COUNT/CHANNEL, ARBITRARY
200
400
600
800
1000
1200
1400
eV

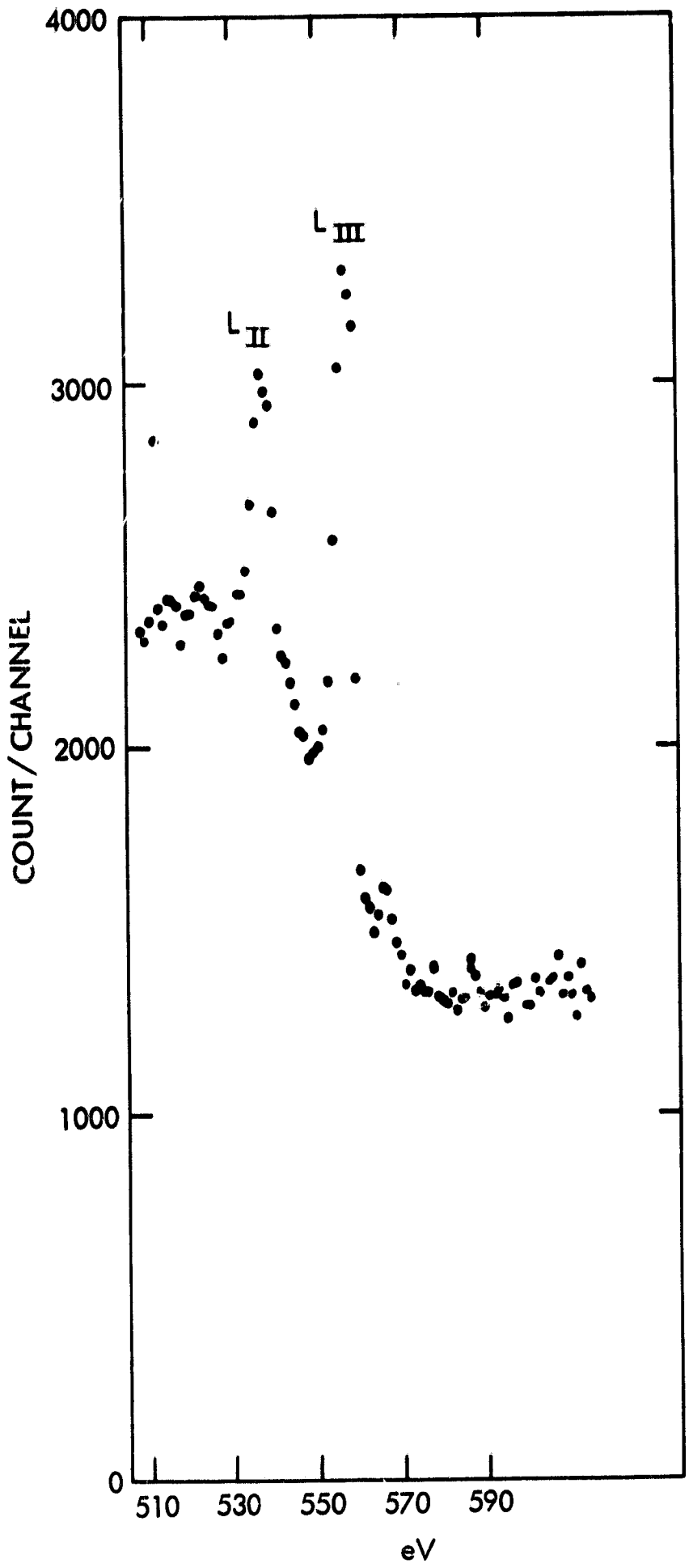
4000
3000
2000
1000
0
COUNT/CHANNEL
L III
L II
510
530
550
570
590
eV

FIG. 3

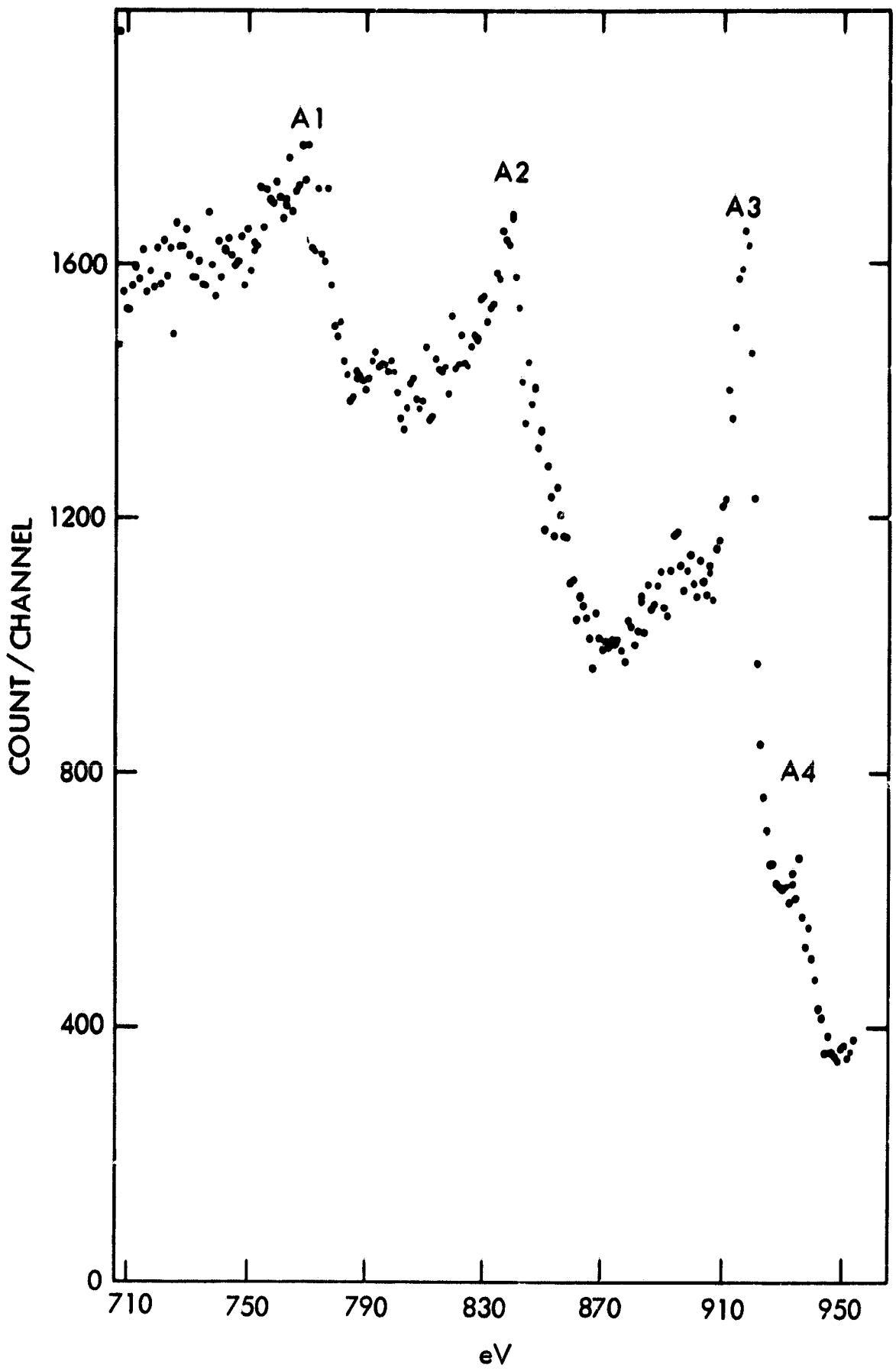
A1
A2
A3
A4
1600
1200
800
400
0
COUNT/CHANNEL
710
750
790
830
870
910
950
eV

FIG. 4

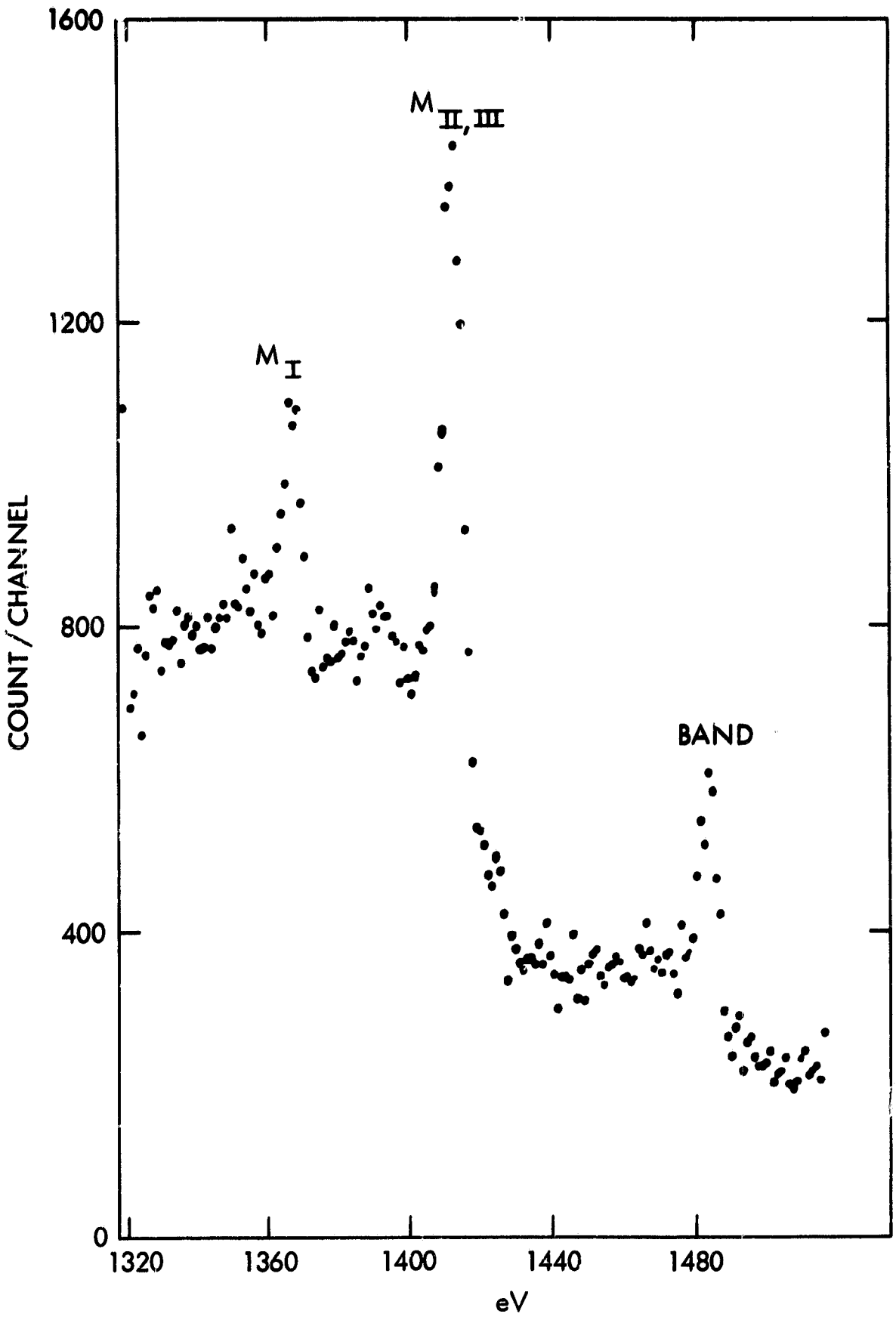
1600
1200
800
400
0
COUNT / CHANNEL
M II, III
M I
BAND
1320
1360
1400
1440
1480
eV

FIG. 5

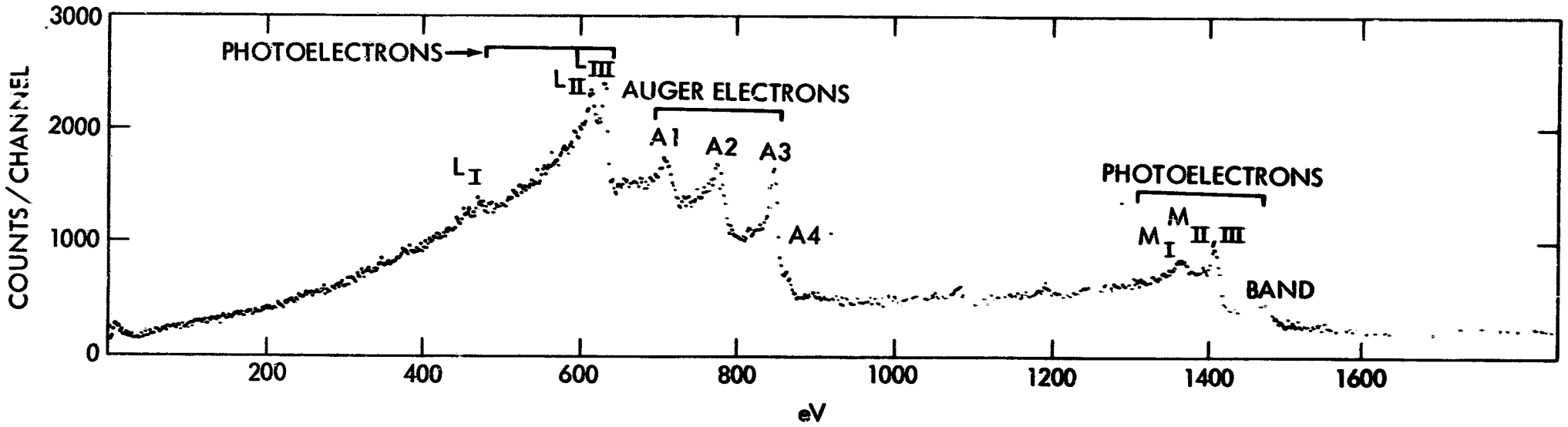
3000
2000
1000
0
COUNTS/CHANNEL
PHOTOELECTRONS
L_{III}
L_{II}
AUGER ELECTRONS
A1
A2
A3
A4
L_I
PHOTOELECTRONS
$M_{II,III}$
M_I
BAND
200
400
600
800
1000
1200
1400
1600
eV

FIG. 6

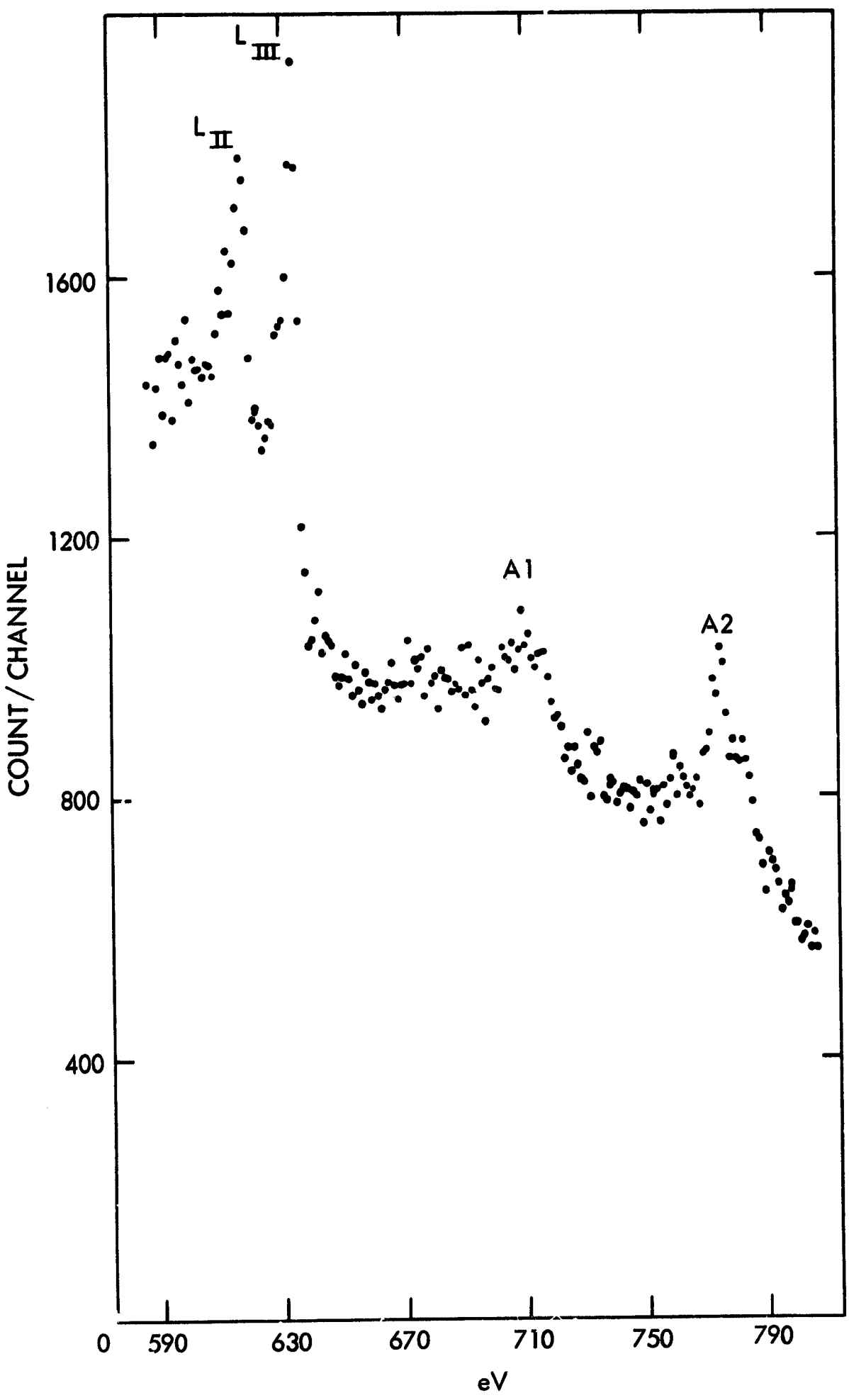
L III
L II
1600
1200
800
400
COUNT/CHANNEL
A1
A2
0
590
630
670
710
750
790
eV

FIG. 7

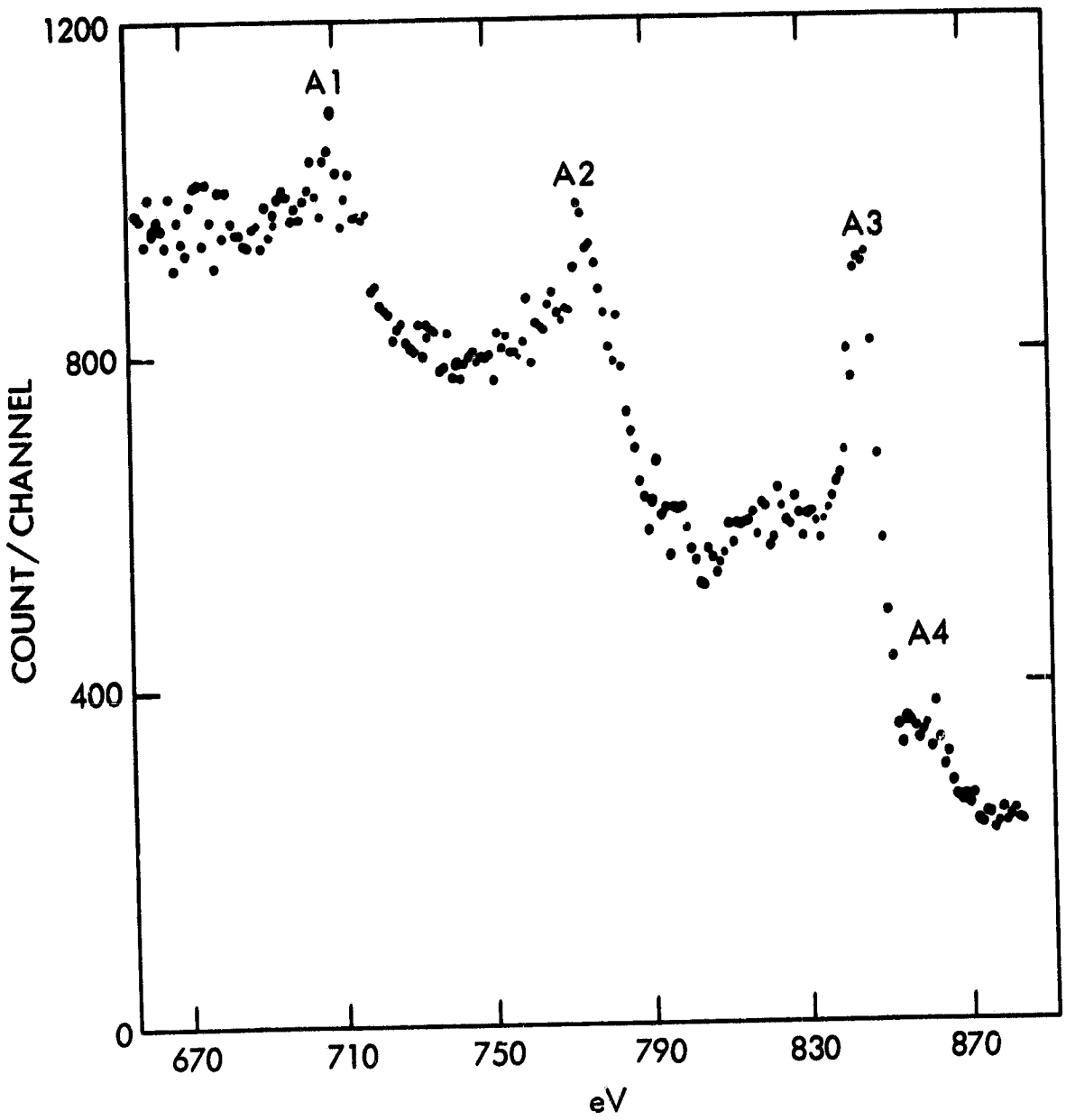
1200
800
400
0
COUNT/CHANNEL
A1
A2
A3
A4
670
710
750
790
830
870
eV

FIG. 8

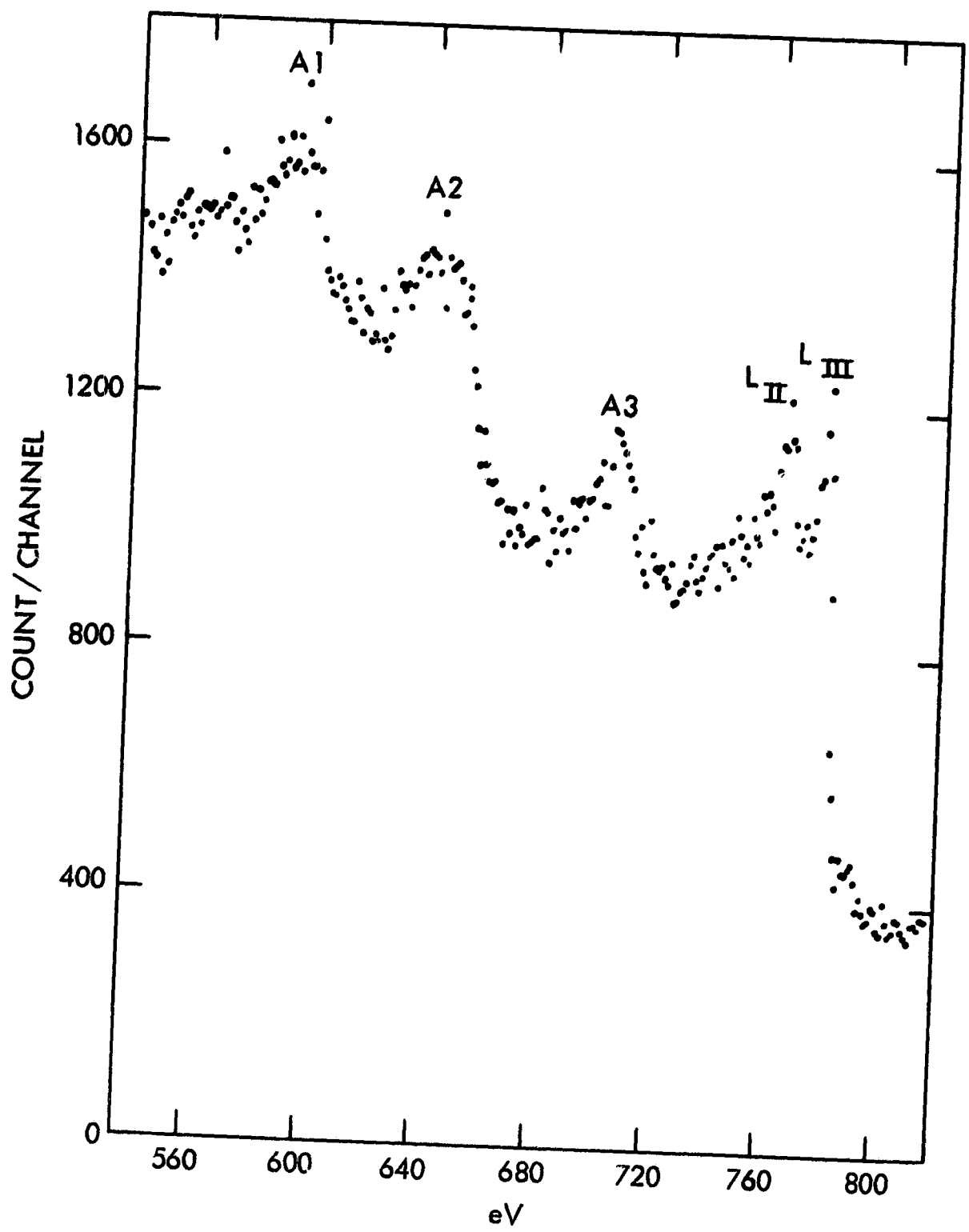
A1
A2
A3
L II
L III
1600
1200
800
400
0
COUNT/CHANNEL
560
600
640
680
720
760
800
eV

FIG. 9